Scientia Iranica, Vol. 12, No. 2, pp 131 1

SCIENTIA
IRANICA

Volume-of-Fluid Interface Tracking with Lagrangian Propagation for Incompressible Free Surface Flows

A.H. Nikseresht[1], M.M. Alishahi[*] and H. Emdad[1]

One of the most powerful methods to implement the free surface is the Volume Of Fluid (VOF). In this study, an algorithm is developed, which includes an implicit pressure based method (SIMPLE) with a staggered grid and a Lagrangian propagation VOF method. Based on this algorithm, a computer code is generated and a cavity with a free surface and two test cases of dam-breaking problems are examined and, then, the effect of fluid sloshing on a near wall is also analyzed and a time history of the normal force on the wall is presented. The results show good agreement with experimental and other computational results.

INTRODUCTION

Incompressible viscous flows with moving free surfaces are instances which occur both in industry and in nature, such as in environmental engineering, die-casting, injection molding processes, marine sciences and many others. Available numerical methods for such problems can be classified into moving and fixed grid approaches. The moving grid approach is, typically, confined to special applications, due to limitations in the rezoning technique [1-3]. In this connection, the fixed grid approach seems to be a more viable method, whenever a general motion of free surface flow is considered [4,5].

Among the existing fixed grid approaches, Harlow and Welch [6] proposed the well-known marker and cell method (MAC) that labels fluid particles with markers. Recently, Nakayama and Mori [7] improved the MAC method to preclude the possibility of producing an unphysical liquid front advancement. In the MAC method, the region occupied by the fluid is tracked by the locations of the markers in the course of fluid motion. Such a method defines the fluid region rather than the free surface and, thus, requires large computer storage and additional computational time to move all fluid markers to new locations, especially when a three-dimensional problem is encountered [8]. Furthermore, a finite volume far from the free surface might be unrealistically overfilled or partially filled with markers, due to numerical error. In 1981, Hirt and Nichols [9] introduced the Volume Of Fluid method (VOF) for incompressible flow with a moving free surface.

In the VOF method, which the interface describes implicitly, the data structure that represents the interface is the fraction, C, of each cell that is filled with a reference phase, say phase 1. The scalar field, C, is often referred to as the color function. The magnitude of C in the cells cut by the free surface is between 0 and 1 ($0 < C < 1$) and, away from it, is zero or one. The data C are given at the beginning of a computational cycle, but no approximation of the interface position is known. The method is implicit, since one needs to "invert" the data, C, to find the approximate interface position. In other words, an algorithm for interface reconstruction is needed. Typically, one can reconstruct the interface by the straightforward Simple Line Interface Calculation (SLIC) method [10] or by various "Piecewise Linear Interface Calculation" (PLIC) methods [11]. The latter methods give much better results than the former. The advantages of the VOF method are as follows:

1. It preserves mass in a natural way, as a direct consequence of the development of an advection algorithm, based on a discrete representation of the conservation law;

2. No redistribution of the surface markers is necessary when they are stretched by the flow and no special

1. *Department of Mechanical Engineering, Shiraz University, P.O. Box 3474, Shiraz, I.R. Iran.*
*. *Corresponding Author, Department of Mechanical Engineering, Shiraz University, P.O. Box 3474, Shiraz, I.R. Iran.*

provision is necessary to perform reconnection of the interfaces;

3. It can be relatively simply extended from two-dimensional to three-dimensional domains;
4. The scheme is local in the sense that only the C values of the neighboring cells are needed to update the C value in a cell. For this reason, it is relatively simple to implement these algorithms in parallel, in particular within the framework of domain decomposition techniques.

In incompressible Computation of Fluid Dynamics (CFD), the leading class of techniques for the numerical solution of pressure is the SIMPLE class of methods, as formulated by Patankar [12,13]. Unfortunately, very few papers have investigated the application of the SIMPLE algorithm to free surface flow modeling. This is in contrast to the fact that most of the world-wide leading CFD workers use these methods. In the present paper, the appropriate numerical technique is introduced to solve the Navier Stokes equations, for a two-phase incompressible flow with a high density difference. Performance of the proposed numerical procedure will be examined through the solution of a cavity with a free surface and two, well-documented, dam-breaking examples. Then, a wall near the broken-dam is considered and the impingement of the flow on the wall is analyzed and the normal forces at different times are presented.

GOVERNING EQUATIONS

Let $\vec{U}$ be the velocity vector field, ρ the density, p the pressure and μ the viscosity. Then, the Navier-Stokes equations are:

$$\partial_t(\rho\vec{U}) + \nabla.(\rho\vec{U}\otimes\vec{U}) = -\nabla p + \nabla.(2\mu D) + \rho\vec{g}, \quad (1)$$

where D is the rate-of-strain tensor with components:

$$D_{ij} = \frac{1}{2}\left(\frac{\partial U_j}{\partial x_i} + \frac{\partial U_i}{\partial x_j}\right). \quad (2)$$

Viscosity and density are assumed to be constant in each phase, but may vary from phase to phase. μ_i and ρ_i are the viscosity and density in phase i, respectively. These equations may be viewed as a "one-fluid formulation", as they are expressed at any position, $\vec{X}$. Consider incompressible fluids, with:

$$\nabla.\vec{U} = 0.0. \quad (3)$$

If these equations were transformed to a dimensionless form as follows:

$$x = \frac{x}{L}, \qquad y = \frac{y}{L}, \qquad u = \frac{U_i}{U_\infty},$$
$$v = \frac{U_j}{U_\infty}, \qquad p = \frac{P-P_\infty}{\rho_L U_\infty}, \qquad \rho^* = \frac{\rho}{\rho_L},$$
$$\mu^* = \frac{\mu}{\mu_L}, \qquad \tau = \left(\frac{U_\infty}{L}\right)t, \qquad \mathrm{Re} = \frac{\rho_L U_\infty L}{\mu_L},$$

where L is an arbitrary characteristic length and ρ_L, μ_L stands for Liquid density and viscosity, respectively, then, a single set of governing equations, covering both the liquid and the surrounding air, could be written as:

$$\rho^*\left(\frac{\partial u}{\partial \tau} + u\frac{\partial u}{\partial x} + v\frac{\partial u}{\partial y}\right) = -\frac{\partial p}{\partial x} + \frac{\mu^*}{\mathrm{Re}}\nabla^2 u, \quad (4)$$

$$\rho^*\left(\frac{\partial v}{\partial \tau} + u\frac{\partial v}{\partial x} + v\frac{\partial v}{\partial y}\right) = -\frac{\partial p}{\partial y} - \rho^*\frac{1}{\mathrm{Fr}^2} + \frac{\mu^*}{\mathrm{Re}}\nabla^2 v, \quad (5)$$

where $Fr = \frac{U_\infty}{\sqrt{gL}}$ is the Froude no. and density ρ^* and viscosity μ^* are step functions across the free surface. They are unity in the liquid region and jump to another constant in the air region, i.e.:

$$\rho^* = \left\{\begin{matrix} 1 & \text{in liquid} \\ \frac{\rho_a}{\rho_L} & \text{in air}\end{matrix}\right\}, \qquad \mu^* = \left\{\begin{matrix} 1 & \text{in liquid} \\ \frac{\mu_a}{\mu_L} & \text{in air}\end{matrix}\right\}.$$

Another useful formulation is: If χ is a characteristic function with value 1 in phase 1 and 0 in phase 2, then, the equation governing the change of χ, following the motion of the fluid, is [14,15]:

$$\partial_t\chi + u.\nabla\chi = 0.0. \quad (6)$$

The color function, C, in the VOF method may be viewed as a discretization of the characteristic function. μ^* and ρ^* at any cells (denoted by ij) can be computed using a simple volume average over the cell:

$$\rho^*_{ij} = C_{ij}\rho^*_L + (1-C_{ij})\rho^*_a, \quad (7)$$

$$\mu^*_{ij} = C_{ij}\mu^*_L + (1-C_{ij})\mu^*_a. \quad (8)$$

A more explicit account of the interface should be taken, considering the special nature of the problem, which is introduced in the following.

INTERFACE TRACKING

In the PLIC, at each time step, given the volume fraction of one of the two fluids in each computational cell and an estimate of the normal vector to the interface, a planar surface is constructed within the cell with a unique normal vector and the cell is divided into two parts, each of which contains the proper

area of one of the two fluids. This interface is, then, propagated by the flow and the resulting area of each fluid into its neighboring cells is determined. The updated values of the area fraction fields are found throughout the domain and the numerical simulation can proceed to the next time step. The next three subsections describe the procedure for estimating the normal vector, the construction of the interface in each cell and the propagation of the interface by the flow.

Normal Estimation

The reconstruction is based on the idea that a normal vector, $\vec{m}$, together with the fractional volume, C, determines a unique line interface cutting the cell. In the first part of the reconstruction, a normal direction to the interface is estimated, using a finite-difference formula. The normal vector is defined as:

$$\vec{m} = \nabla C. \tag{9}$$

At first, a cell corner value of the normal $\vec{m}$ vector is computed at $(i+1/2, j+1/2)$ by:

$$m_{x,i+1/2,j+1/2} = \frac{1}{2\Delta x}(C_{i+1,j} - C_{i,j} + C_{i+1,j+1} - C_{i,j+1}), \tag{10}$$

$$m_{y,i+1/2,j+1/2} = \frac{1}{2\Delta y}(C_{i,j+1} - C_{i,j} + C_{i+1,j+1} - C_{i+1,j}). \tag{11}$$

Then, the required cell centered values are computed from the cell corner values by averaging:

$$m_{ij} = \frac{1}{4}(m_{i+1/2,j-1/2} + m_{i-1/2,j-1/2} + m_{i+1/2,j+1/2} + m_{i-1/2,j+1/2}). \tag{12}$$

If ∇^h is a difference operator for the gradient, it can be seen from Equation 12 that ∇^h will be approximated from nine neighboring points.

Connecting Fractional Volume and Interface Position

In the second part of the reconstruction, a line interface, which divides the computational cell into two parts containing the proper area of each fluid, must be found. This is achieved by deriving an explicit expression, which relates the "cut" area to a parameter, α, which completely defines the interface. The problem can be started as follows: Given a rectangular (or square) cell of sides c_1 and c_2 in the (x_1, x_2) plane, depicted in Figure 1 and a straight line (such as EH) with normal vector $\vec{m}$, find the area of the region (ABFGDA). To obtain an expression for this area, let

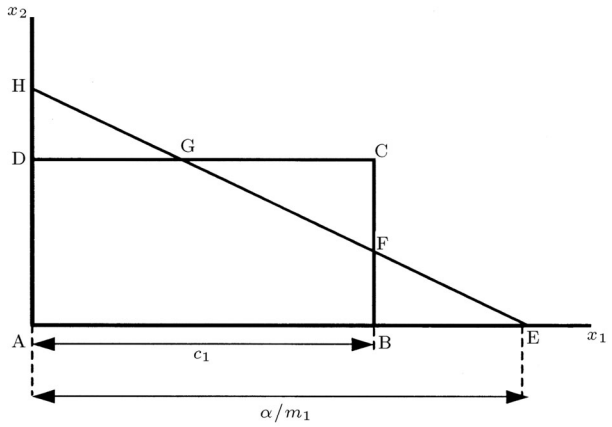

Figure 1. The "cut area" refers to the region within the rectangle ABCD which also lies below the straight line EH, having normal m and parameter α.

one suppose that the components m_1 and m_2 of the normal vector are both positive. The most general equation for the straight line in the (x_1, x_2) plane with normal $\vec{m}$ is:

$$m_1 x_1 + m_2 x_2 = \alpha. \tag{13}$$

The area of the region contained below this line, within the rectangle $ABCD$, is given by:

$$\text{Area} = \frac{\alpha^2}{2m_1 m_2}\left[1 - H(\alpha - m_1 c_1)\left(\frac{\alpha - m_1 c_1}{\alpha}\right)^2 - H(\alpha - m_2 c_2)\left(\frac{\alpha - m_2 c_2}{\alpha}\right)^2\right]. \tag{14}$$

The prefactor, $\alpha^2/2m_1m_2$, on the right-hand side of this equation, is simply the area of the triangle, AEH. In case points E and H lie within the original rectangle, this is the desired area. If point E is to the right of point B, i.e., if $\alpha \rangle m_1 c_1$, the area of the small triangle, BEF, must be subtracted to obtain the proper area. Since triangle BEF is geometrically similar to triangle AEH, the ratio of their areas is equal to the square of the ratio of the sides BE to AE, given by:

$$\frac{\text{Area of } BEF}{\text{Area of } AEH} = \left(\frac{\alpha/m_1 - c_1}{\alpha/m_1}\right)^2 = \left(\frac{\alpha - m_1 c_1}{\alpha}\right)^2.$$

This corresponds to the second term within the square brackets on the right-hand side of Equation 14, which also contains the Heaviside step function, $H(\alpha - m_1 c_1)$, defined, such that:

$$H(x) = \begin{cases} 0 & \text{for } x < 0 \\ 1 & \text{for } x > 0 \end{cases}.$$

Since the area of the triangle, BEF, is only subtracted if E is to the right of B. Similarly, the third term

within the square brackets in Equation 14 subtracts the area of the triangle, DGH, provided that point H lies above point D, i.e., if $\alpha > m_2c_2$. The single formula (Equation 14), thus, provides the area of the region below the straight-line (Equation 13), which lies in the original rectangle of sides c_1 and c_2, for all possible cases. The area is a continuous, one-to-one, monotonically increasing function of α. It ranges from zero, when $\alpha = 0$, to c_1c_2, when α reaches its maximum value of $m_1c_1 + m_2c_2$.

In practice, not only does one need the forward relation (Equation 14) between the cut area and the parameter, α, but, the method also requires the inverse problem of determining α, which corresponds to a given cut volume and normal direction in a computational cell. One can simply use a standard iterative root-finding approach. Another option, which is the one that is implemented here, is as follows: Corresponding to each critical value of α, for which the interface passes through one of the corners of a rectangle, there exists a critical value of the cut area. Between any two critical values, the roots of function (Equation 14) can be evaluated analytically.

Lagrangian Propagation of the Interface Segments

Once the interface has been reconstructed, its motion, by the underlying flow field, must be modeled by a suitable advection algorithm. This can be achieved by either an Eulerian or a Lagrangian scheme. In the Eulerian method, one computes the fluxes of χ across the faces of the control volume, V_{ijk}. The characteristic function, χ, is conserved in an incompressible flow and the flux, during time τ, across the face F of V_{ijk}, is:

$$\phi_F = \int_F \int_{t_n}^{t_n+\tau} \chi u.n' dF dt, \tag{15}$$

where n' is the unit normal vector to the face. This expression may be estimated, once the area of face F that is "wetted" by phase 1, is found from the reconstruction algorithm of the previous section. The explicit evaluation of the time integral forms the basis of the Eulerian method. The Lagrangian approach to the propagation of the interface can be best described by considering the way in which the given interface (Equation 13) is propagated by the flow [14,15]. For this purpose, rewrite Equation 11 with superscript (n) attached to all the variables,

$$m_1^{(n)}x_1^{(n)} + m_2^{(n)}x_2^{(n)} = \alpha^{(n)}, \tag{16}$$

and think of this as the equation for the interface in the given cell at the initial time, t_n. The Lagrangian advection of this interface by the flow, as time increases to $t_{n+1} = t_n + \tau$, will modify it to a new form, which must be calculated. Since, in practice, the time stepping is performed separately in each spatial direction through operator splitting, the advection of the interface along only one spatial coordinate, say x_1, will be described.

To make the description simpler, let one suppose that the left face of the cell has coordinate $x_1 = 0$ and the right face $x_1 = h = c_1$. Also, denote the x_1 components of the velocity on the faces by U_0 and U_h. These are taken to be constant over the entire face to which they are assigned. The x_1 component of the velocity, within the cell, is a simple linear interpolation of the form:

$$u_1(x_1) = U_0\left(1 - \frac{x_1}{h}\right) + U_h\frac{x_1}{h}. \tag{17}$$

For each point initially at $x_1^{(n)}$, the above velocity is calculated and assumed to remain constant in time during the advection step. Then, the x_1 coordinate of each point initially on the interface (Equation 16) changes to the new value:

$$x_1^{(*)} = x_1^{(n)} + u_1(x_1^{(n)})\tau$$

$$= \left[1 + \left(\frac{U_h - U_0}{h}\right)\tau\right] x_1^n + U_0\tau. \tag{18}$$

The x_2 coordinate remains constant during advection along x_1. The superscript $(*)$ is used rather than $(n+1)$ to denote a fractional step, to be followed by similar steps in the x_2 direction before the advection to time t_{n+1} is completed. In order to find the equation for the interface after this advection step, an expression of $x_1^{(n)}$ in terms of $x_1^{(*)}$ is obtained from Equation 18:

$$x_1^{(n)} = \frac{x_1^{(*)} - U_0\tau}{1 + ((U_h - U_0)/h)\tau}. \tag{19}$$

Upon substituting this result into Equation 16, the interface equation after advection is:

$$m_1^{(n)}\left[\frac{x_1^{(*)} - U_0\tau}{1 + ((U_h - U_0)/h)\tau}\right] + m_2^{(n)}x_2^{(n)} = \alpha^{(n)}, \tag{20}$$

which can be written in the more standard form:

$$m_1^{(*)}x_1^{(*)} + m_2^{(*)}x_2^{(*)} = \alpha^{(*)}, \tag{21}$$

in which, at x_1 direction;

$$m_1^{(*)} = \frac{m_1^{(n)}}{1 + ((U_h - U_0)/h)\tau}, \qquad m_2^{(*)} = m_2^{(n)}, \tag{22}$$

$$\alpha^{(*)} = \alpha^{(n)} + \frac{m_1^{(n)}U_0\tau}{1 + ((U_h - U_0)/h)\tau}. \tag{23}$$

After advection, one has to check whether the interface has protruded at all into the neighboring cells to the right and left and, if so, to calculate the volumes moved into those cells. Thus, for instance, if $\alpha^{(*)}/m_1^{(*)}$ is larger than h, a portion of the volume originally contained below (Equation 16), has moved to the right cell. This area can be calculated using the general formula (Equation 14), provided that the equation for the interface is rewritten in an appropriate form by making one additional coordinate transformation in Equation 21. Let:

$$x_1^{(*)} = h + x_1', \tag{24}$$

so that x_1' measures distances from the left face, $x_1 = h$, of the right cell. With this substitution, Equation 16 becomes:

$$m_1^{(*)} x_1' + m_2^{(*)} x_2^{(*)} = \alpha', \tag{25}$$

where:

$$\alpha' = \alpha^{(*)} - m_1^{(*)} h. \tag{26}$$

Using the coefficients of Equation 25, Formula 14 can now be used to calculate the area of the phase 1 fluid that was moved to the right neighboring cell. Similarly, if U_0 is negative, the volume moving to the left neighboring cell can be calculated. Finally, the volume, which remains in the original cell, is calculated, using Equation 16 and Formula 14, provided that account is taken of the change in the size of the parallelepiped, which results if U_0 is positive and/or U_h is negative. In particular, if U_0 is positive, the left face moves in by an amount, $U_0\tau$, during time interval τ and, to calculate the volume remaining in the cell, it is necessary to make a coordinate transformation similar to Equation 24, which puts the origin on this new left face.

To illustrate the method, the procedure is sketched in Figure 2. The shaded region represents the volume lost by the original cell and gained by the downwind cell. Formula 14, applied to parallelepiped $AEFB$, can be used to calculate the volume of the shaded region. With this procedure, the volume fraction field is updated at time t_{n+1}.

This Lagrangian method is stable and satisfies the physical constraint on the volume fraction, $0 \leq C \leq 1$, when the CFL condition, $(\max|u|)\tau/h < 1/2$, is satisfied. The programming of the Lagrangian method is considerably simplified by the fractional-step strategy, described above.

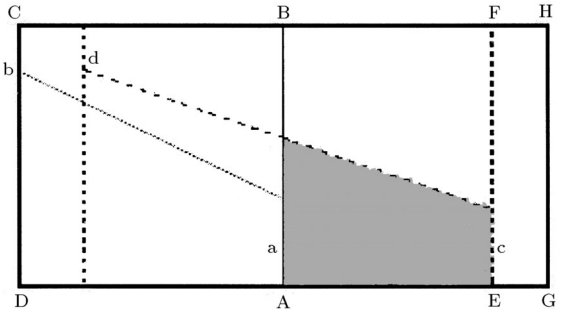

Figure 2. A schematic illustration of the Lagrangian propagation of the interface in two dimensions.

NUMERICAL PROCEDURE

The algorithm follows these steps:

a) Initialize the flow field variables and, then, the numerical procedure, in one time step, is as follows:

b) Propagate the volume fraction for the new time step, based on the velocity from the previous time step and update phase averaged quantities by the following sub steps:

   1) Normal estimation,
   2) Reconstructing the interface,
   3) Propagating the interface,
   4) Compute new values of C and other averaged quantities.

c) Use the SIMPLE algorithm to solve the flow field governing equations;

f) Repeat b-c.

RESULT AND DISCUSSION

At first, a two-dimensional cavity with fixed vertical side walls, a driven floor and a free surface at the upper boundary was modeled; the geometry is shown in Figure 3. Results were obtained for flows with a Reynolds number of 100 and for Froude numbers varying between 0.2 and 2.0.

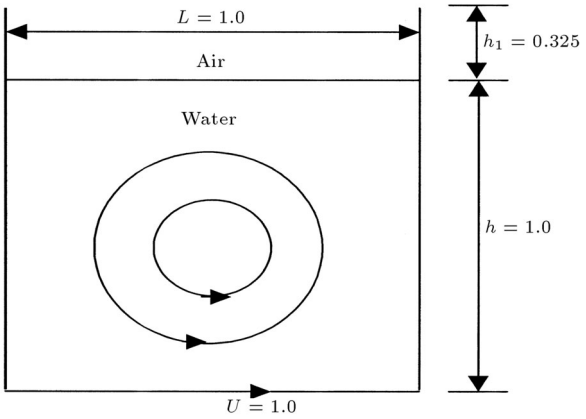

Figure 3. The geometry for the free surface driven cavity problem.

The stream functions for the free surface flow, at a Froude number of 2.0, is shown in Figure 4 and are compared with the stream functions for a conventional driven cavity (Figure 5), where a no-slip stationary wall, at the same Reynolds number, replaces the top surface. It is readily seen that, for the free surface problem, the surface has been displaced by the flow and no longer lies on the horizontal plane. Also, the two recirculation bubbles in the top corner, for the conventional cavity, are missing. These two features are due to the lack of restraining shear force upon the upper boundary.

The effect of the Froude number on the free surface elevation is shown in Figure 6 and is compared with the results of the MAC method [16]. As the Froude number increases, the disturbance in the free surface position grows, where the elevation of the free surface is seen to be proportional to the square of the Froude number, which is consistent with physical reasoning.

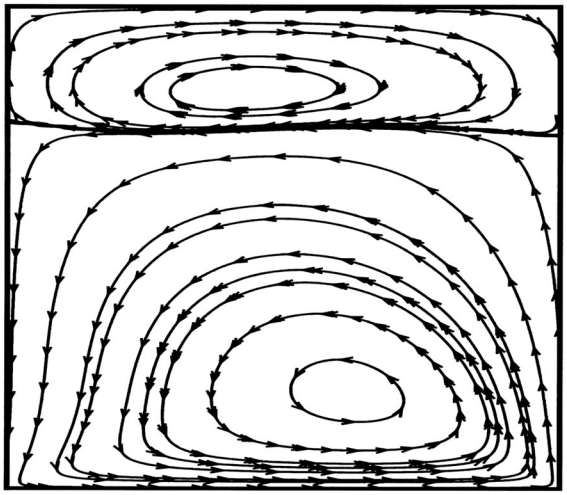

Figure 4. The streamlines for a floor driven cavity with a free surface (Re = 100 and Fr = 2).

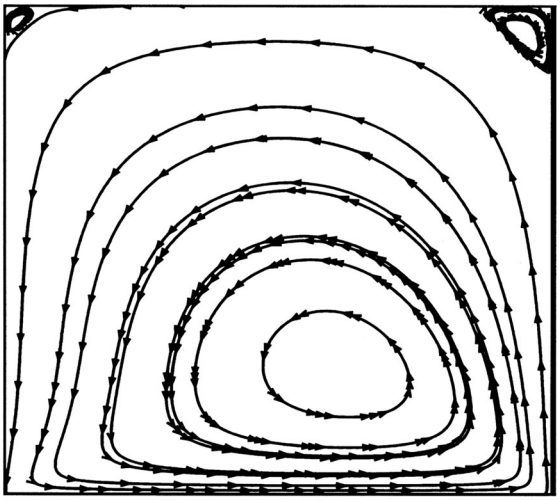

Figure 5. The streamlines for a conventional floor driven cavity (Re = 100).

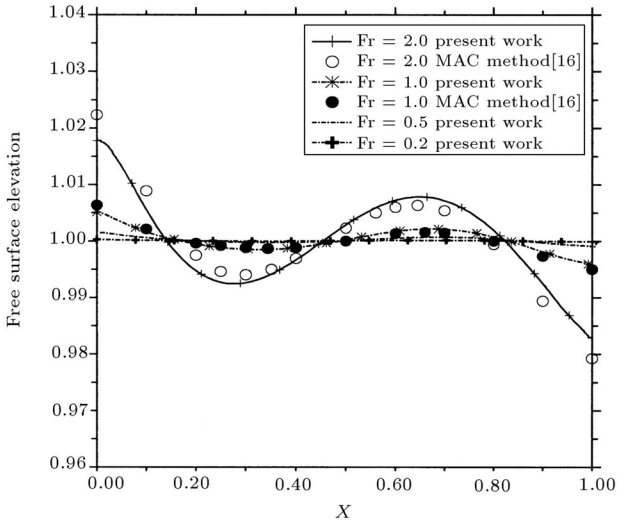

Figure 6. The free surface elevation for the driven cavity, calculated for a flow with Re = 100 on a 129 * 169 mesh.

To demonstrate the mesh independence of the free surface flow, solutions of the free surface profile, for a cavity with Froude number 2.0, is shown in Figure 7. As the mesh is refined, the free surface elevation converges towards a mesh independent position. To examine the performance of the present numerical procedure, two cases of the dam-breaking problem are considered at this point. Water and air are adopted as the media of the flow. The height and width of the water column of the two cases are (2.25 in, 2.25 in) and (4.5 in, 2.25 in) and corresponding Reynolds numbers, in terms of the height of the liquid region, are 43,129 and 121,986, respectively. In most free surface flows, the grid near the free surface should be fine,

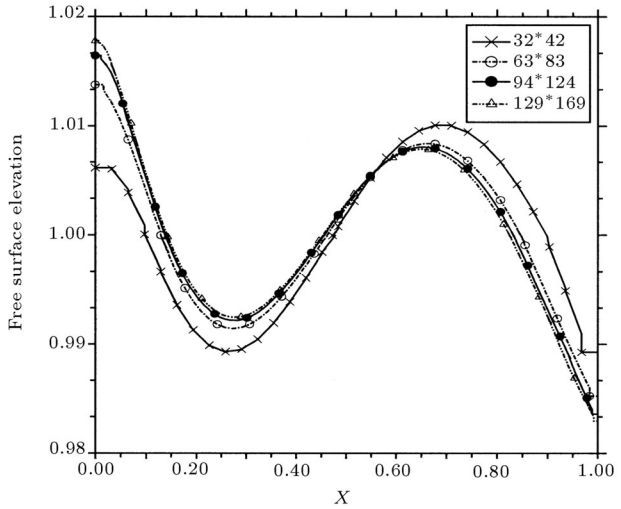

Figure 7. Convergence of the calculated free surface with Fr = 2 and Re = 100 for a range of different meshes.

but, at applications such as dam-breaking, since the flow sweeps through a great part of the domain at all possible inclinations, it is better to use fine grids in the entire flow field. Thus, for simplicity, a uniform Cartesian grid system, $\Delta x_i = \Delta x = \Delta y_i = \Delta y$, is used. In the case of (2.25 in, 2.25 in), three grids, namely, $81 \times 41, 101 \times 51$ and 201×101 grid points are employed on the dimensionless domain of $0 \leq x \leq 4$ and $0 \leq y \leq 2$, which means the grid sizes of $\Delta x = \Delta y = 0.05, 0.04$ and 0.02, respectively. Figure 8 shows the isobar and velocity vector of the first case (2.5 in * 2.5 in) at various time steps and it is obvious that the pressure is, essentially, near zero in the air region. This can be attributed to the negligible density of the air, as compared to the water. It is interesting to note from velocity vectors that the conservative Equations 1 to 3 induce a vortex in the layer of air adjacent to the free surface, which is consistent with physical reasoning.

Figure 9 shows the resulting water front, $x_f(\tau)$, of the present study on various grids for the case of a square water column, $H = W = 2.25$ in. The available experimental data [17] and the existing numerical results, such as the standard MAC method [6] and the modified MAC method [7], are also plotted in Figure 9. As shown in this figure, MAC methods overpredict the experimental results, but, the present work shows much better agreement with experiments.

In the second case of (4.25 in * 2.25 in), two grids,

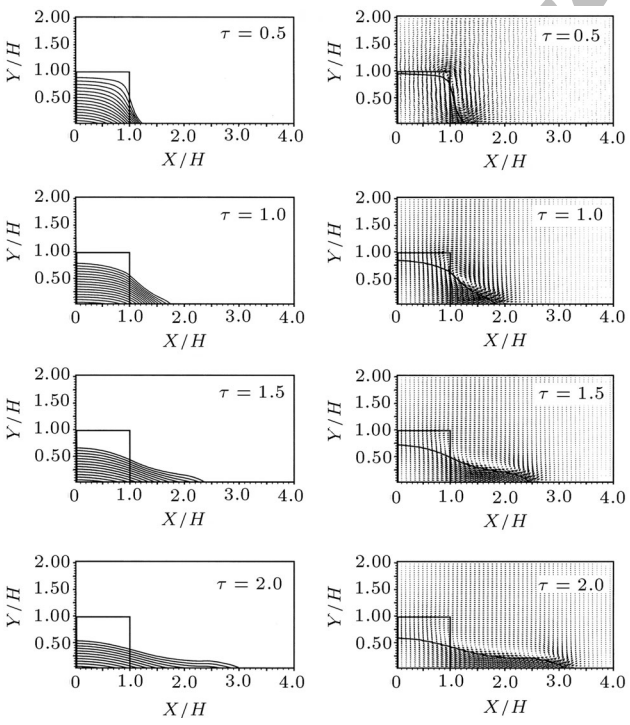

Figure 8. Isobars with increment of $\Delta p = 0.05$ and velocity vectors at various times for the case of (2.5 in * 2.5 in).

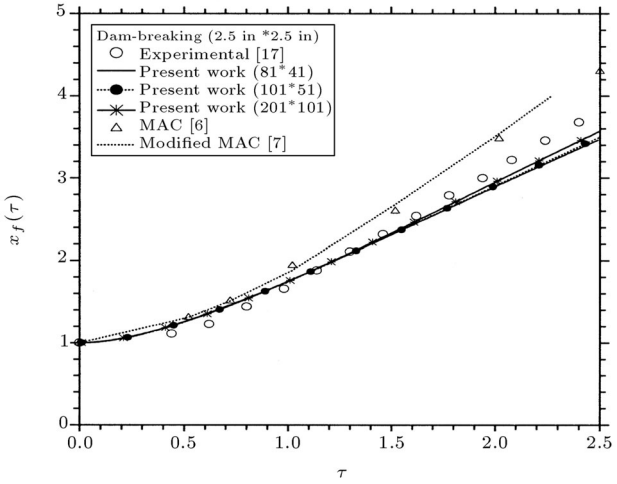

Figure 9. Comparison of the waterfront, $x_f(\tau)$, from the present results, experimental data and other existing numerical results for the case of (2.5 in * 2.5 in).

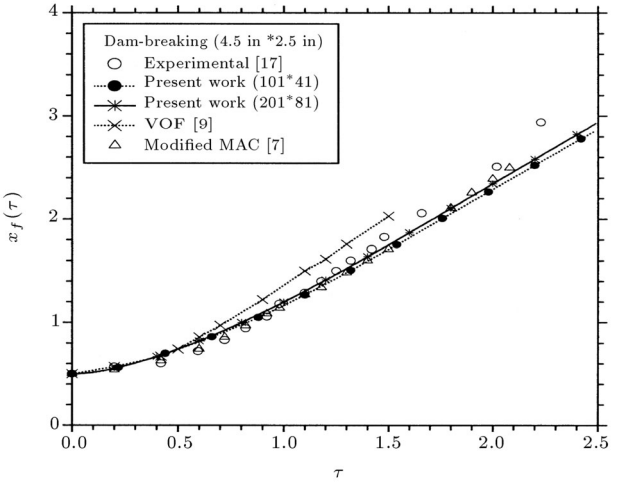

Figure 10. Comparison of the waterfront, $x_f(\tau)$, from the present results, experimental data and other existing numerical results for the case of (4.5 in * 2.5 in).

namely, 101×41 and 201×81 grid points, are employed on the dimensionless domains of $0 \leq x \leq 10/3$ and $0 \leq y \leq 4/3$. Figure 10 shows a comparison of the waterfront from different sources. It includes the results of the present work, the previous VOF code of Hirt and Nicholls [9] and the modified MAC method. It is obvious from Figure 10 that the Hirt and Nichols code [9] overpredicts the experimental data. The MAC results are more comparable with the experimental data in Figure 10 than those of Figure 9; however, comparison of the present results with experimental results are almost the same in both cases.

At last, the force extended by a broken dam on a nearby wall, is analyzed. A wall is set at a distance of 1.5 H from a dam. Figure 11 shows the dynamic evolution of the liquid configuration at different times. As shown in this figure, at $\tau = 1.8$,

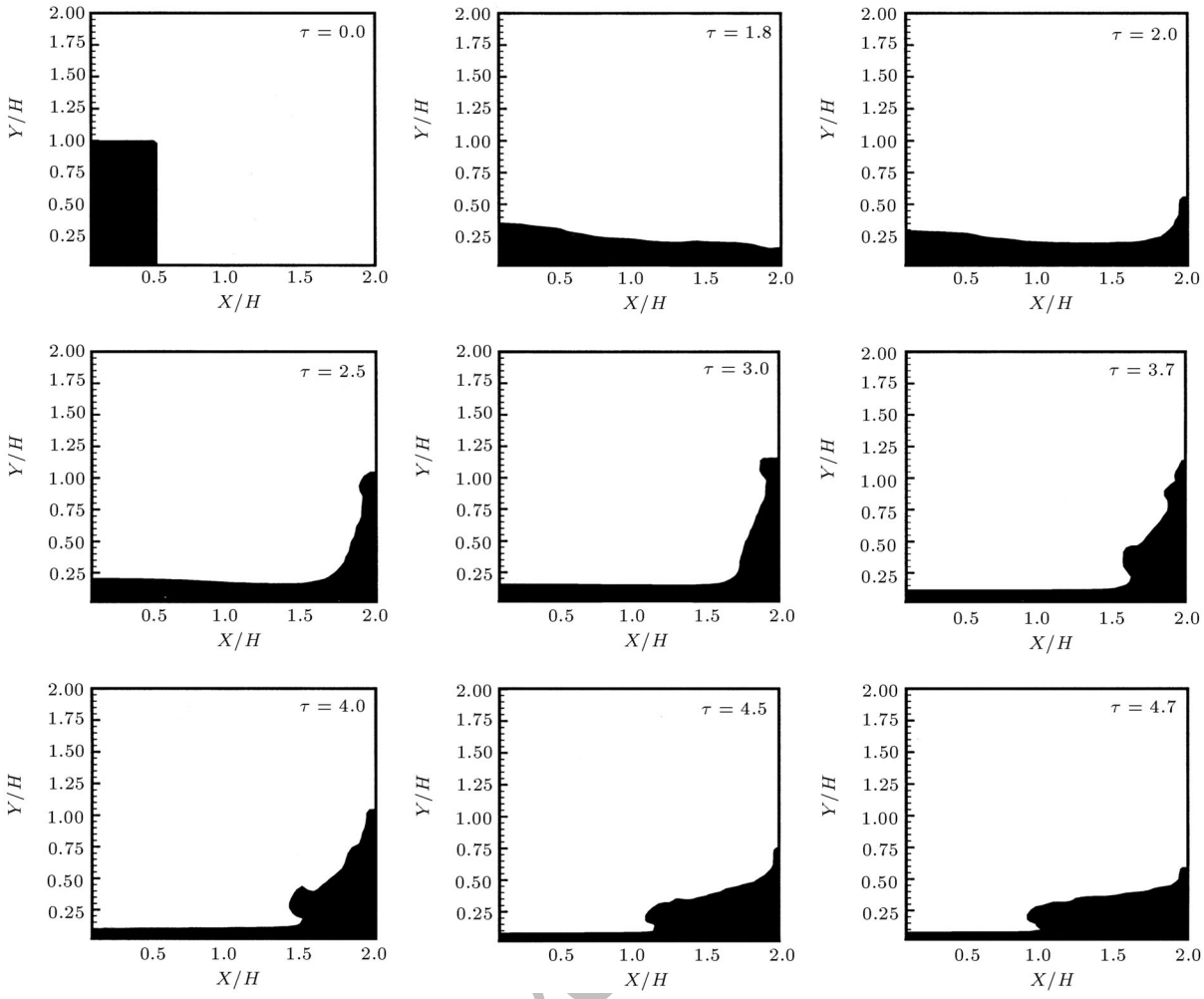

Figure 11. Dynamical evolution of the liquid configuration of a breaking-dam on a nearby wall.

the leading edge of the water column reaches the right wall. The front of the rising water column begins to go down and a breaking wave generates at the bottom at $\tau = 3.7$ to $\tau = 4.0$ and the bore front, generated due to the wave breaking, then, moves to the left wall, at $\tau = 4.5$. The main reason for this wave breaking and the emerging jet (Figure 11, $\tau > 3.7$) is the interaction of two counter flows. One of these flows is coming down from the right wall and the other is due to the remains of the initial flow from left to right. This interaction of two flows and the resulting stagnant region is clearly seen in Figure 11. To examine further details for the dynamical evolution of the breaking wave, please see Figure 12, which represents the velocity vectors in each phase and the interface between the phases at $\tau = 0.0, 3.0, 3.7, 4.5, 4.7$ and 6, respectively. A large circulation structure in the gas phase appears appreciably in front of the liquid phase. Two counter flows mentioned earlier are also seen in Figure 12, $\tau > 3.7$, which produce a stagnation point flow near the bottom wall. It is evident that the dynamical evolution of the breaking wave contains quite complicated behavior in both liquid and gas phases. Figure 13 represents the time history of a normal force coefficient on the wall, ($Cn = \frac{F}{\rho U_\infty^2 H}$). It shows that at $\tau = 2.5$, the force on the lower part of the right wall is maximum, which is mainly due to high static pressure at this location. The forces on the lower part of the right wall, at $\tau = 3.5$, become less than $\tau = 2.5$, but the forces at the upper region of the wall become more than that at $\tau = 2.5$ because of the effect of dynamic pressure. At $\tau = 4.0$ and $\tau = 4.5$, when the flow starts to come down, the forces at all regions go up. When the flow is setting down, the forces, again, start to decrease ($\tau = 4.7$).

CONCLUSION

A single set of dimensionless equations is derived to handle both liquid and air phases in viscous incompressible free surface flows. The momentum equations are solved by the SIMPLE method. The Lagrangian approach is used to solve the VOF method to implement the free surface effect. The results are compared

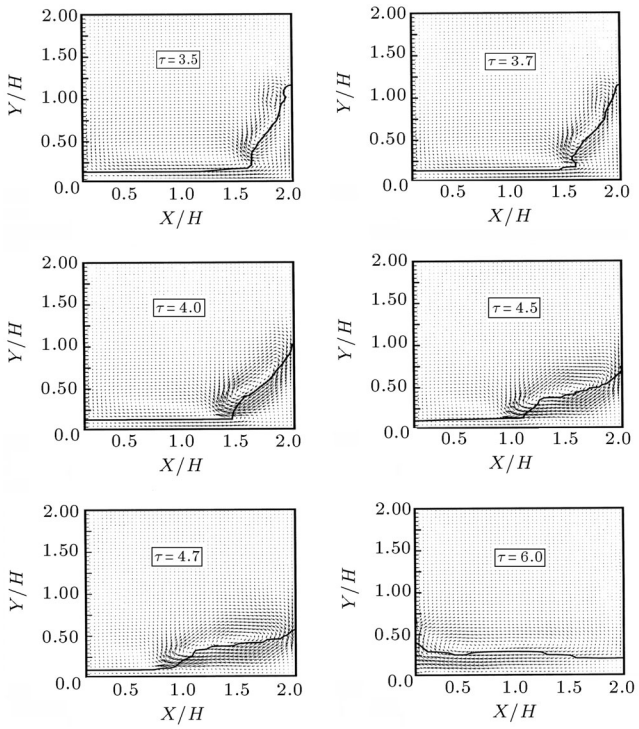

Figure 12. Velocity vectors at various times of a breaking-dam on nearby wall.

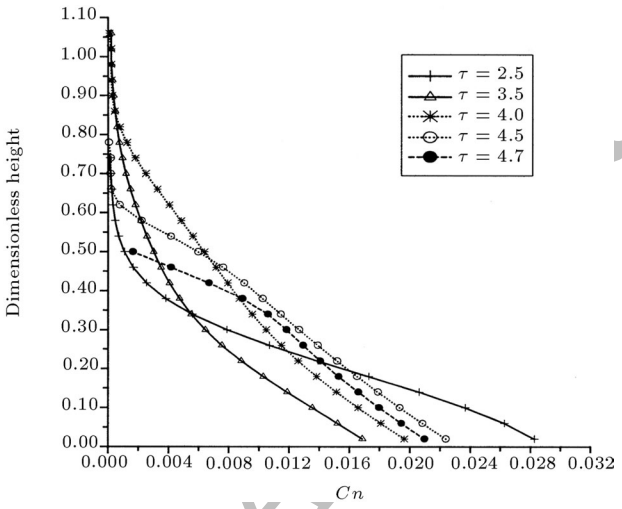

Figure 13. History of normal force coefficients on the right wall at various times.

with two cases of dam-breaking problems, which show good agreement with the experimental data of the waterfront. The algorithm is also applied to a free surface driven cavity problem and the results are compared with those of a closed cavity problem and other numerical methods. Application of the present method to a liquid sloshing problem between two vertical walls reveals the complicated physics of wave breaking and jet emerging in this flow. It can be concluded that the present method and the code is robust and produces results of good quality.

REFERENCES

1. Frits, M.J. and Bories, J.P. "The Lagrangian solution of transient problems in hydrodynamics using a triangular mesh", *J. Comput. Phys.*, **31**, pp 173-215 (1979).
2. Fyfe, D.E., Oran, E.S. and Fritts, M.J. "Surface tension and viscosity with Lagrangian hydrodynamics on triangular mesh", *J. Comput. Phys.*, **76**, pp 349-384 (1988).
3. Lewis, R.W., Navti, S.E. and Taylor, C. " A mixed Lagrangian Eulerian approach to modeling fluid flow during mould filling", *Numer. Meth. Fluids*, **25**, pp 931-952 (1997).
4. Chen, C.W., Li, C.R., Han, T.H., Shei, C.T., Hwang, W.S. and Houng, C.M. "Numerical simulation of filling pattern for an industrial die casting and its comparison with the defects distribution of an actual casting", *Trans. Am. Foundrymen's Soc.*, **104**, pp 139-146 (1994).
5. Shimizu, F., Hatakenaka, K., Tanaka, K., Shigefuji, H. and Shimizu, T. "Numerical analysis of free surface deformation in water tank", *FEDSM2003-45386, Proceedings of ASME FEDSM'03, 4th ASME_JSM Joint Fluids Engineering Conference*, Honolulu, Hawaii, USA (July 6-10, 2003).
6. Harlow, F.H. and Welch, J.E. " Numerical calculation of time dependent viscous incompressible flow of fluid with free surface", *Phys. Fluids*, **8**, pp 2182-2189 (1965).
7. Nakayama, T. and Mori, M. "An Eulerian finite element method for time dependent free surface problems in hydrodynamics", *J. Numer. Meth. Fluids*, **22**, pp 175-194 (1996).
8. Harlow, F.H., Amsden, A.A. and Nix, J.R. "Relativistic fluid dynamics calculations with the particle-in-cell technique", *J. Comput. Phys.*, **20**, pp 119-129 (1976).
9. Hirt, C.W. and Nicholls, B.D. "Volume of fluid (VOF) method for dynamic of free boundaries", *J. Comput. Phys.*, pp 39-201 (1981).
10. Noh, W.F. and Woodward, P. "SLIC (Simple Line Interface Calculation)", *Proceedings, of Fifth International Conference on Fluid Dynamics*, A.I. Vande Vooren and P.J. Zandbergen, Eds., Lecture Notes in Physics, **59**, p 330, Springer-Verlag, Berlin, Germany (1976).
11. Li, J. " Calcul d'interface affine par morceaux (piecewise linear interface calculation)", *C.R. Acad. Sci. Paris, Ser.*, **IIb**, pp 320-391, Paris, France (1995).
12. Patankar, S.V., *Numerical Heat Transfer and Fluid Flow*, Hemisphere, Washington DC, USA (1980).
13. Mousavi Mirkalaee, S.M. "Numerical study of two dimensional laminar incompressible flow around hovercraft", MSc Thesis, Mechanical Engineering, Shiraz University, Iran (Oct. 2001).
14. Gueyffier, D., Li, J., Nadim, A., Scardovelli, R. and Zaleski, S. "Volume-of-fluid interface tracking with smoothed surface stress methods for three-dimensional

flows", *Journal of Computational Physics*, **152**, pp 423-456 (1999).

15. Nikseresht, A.H., Alishahi, M.M. and Emdad, H. "Incompressible Navier-Stokes solution of large scale free-surface flows", *11th Conference (International) of Mechanical Engineering*, Mashhad, pp 158-165 (May 13-15 2003).
16. Norris, S.E. "A parallel Navier-Stokes solver for natural convection and free surface flow", PhD Thesis, Department of Mechanical Eng., Sydney University, (2000).
17. Martin, J.C. and Moyee, W.J. "An experimental study of the collapse of liquid columns on a rigid horizontal plane", *Philos. Trans. Roy. Soc.*, London 244A, pp 312-324 (1952).